Quantum Science and Technology

PURPOSE-LED PUBLISHING™

Coherent and non-unitary errors in ZZ-generated gates

To cite this article before publication: Thorge Müller *et al* 2024 *Quantum Sci. Technol.* in press https://doi.org/10.1088/2058-9565/ad9be2

Coherent and non-unitary errors in ZZ-generated gates

Thorge Müller,[1, 2, *] Tobias Stollenwerk,[3] David Headley,[2, 3] Michael Epping,[1] and Frank K. Wilhelm[2, 3]

[1] *German Aerospace Center (DLR), Institute for Software Technology, Department High-Performance Computing, 51147 Cologne, Germany*
[2] *Theoretical Physics, Saarland University, 66123 Saarbrücken, Germany*
[3] *Institute for Quantum Computing Analytics (PGI 12), Forschungszentrum Jülich, 52425 Jülich, Germany*

(Dated: October 22, 2024)

Variational algorithms such as the Quantum Approximate Optimization Algorithm have attracted attention due to their potential for solving problems using near-term quantum computers. The ZZ interaction typically generates the primitive two-qubit gate in such algorithms applied for a time, typically a variational parameter, γ. Different compilation techniques exist with respect to the implementation of two-qubit gates. Due to the importance of the ZZ-gate, we present an error analysis comparing the continuous-angle controlled phase gate (CP) against the fixed angle controlled Z-gate (CZ). We analyze both techniques under the influence of coherent over-rotation and depolarizing noise. We show that CP and CZ compilation techniques achieve comparable ZZ-gate fidelities if the incoherent error is below 0.03 % and the coherent error is below 0.8 %. Thus, we argue that for small coherent and incoherent error a non-parameterized two-qubit gate such as CZ in combination with virtual Z decomposition for single-qubit gates could lead to a significant reduction in the calibration required and, therefore, a less error-prone quantum device. We show that above a coherent error of 0.04π (2 %), the CZ gate fidelity depends significantly on γ.

I. INTRODUCTION

Quantum computers introduce a novel category of algorithms that cannot be efficiently simulated on classical computers, primarily because of the exponential growth in classical memory demand. Quantum algorithms such as Shor's [1] and Grover's [2] are interesting candidates in the anticipated era of fault-tolerant quantum computing, providing guaranteed asymptotic speedups versus the best-known classical counterparts. In an era of fault-tolerant quantum computers, device error rates fall sufficiently below threshold values, and therefore quantum error correction codes can be utilized. Improvements at all levels are needed to pass this fault-tolerance threshold, from the materials used to fabricate qubits to the on-device layout of physical qubits and the high-order quantum logic performed. Contemporary superconductor-based hardware has attained fidelities for a two-qubit gate in excess of 99 % [3] and, as such, current hardware fidelities come close to the error-threshold [4]. Because of widely spread and popularity, we focus on superconducting platforms and their typical available two-qubit gates. Error sources of two-qubit gates must be analyzed to improve in the coherent and incoherent error regime. In recent years variational quantum algorithms [5, 6] have gained more attention due to their potential to be useful in the NISQ era. Fault-tolerant algorithms, while providing more concrete performance guarantees, are of limited interest as it is unlikely that hardware will advance to enable their use in the near future [7]. Variational NISQ algorithms provide modest hope that with a relatively small number of physical qubits (≈ 100) in the absence of error correction, errors, especially those which are coherent, could be mitigated. This work is structured as follows: First, we give a brief overview of the possible compilation strategies for ZZ-gate into CZ, iSWAP, and CP gates. Second, we introduce error channels included in our study for coherent and incoherent errors. Third and finally, we present numerical and analytical results using error channels for CZ and CP decompositions under differing error conditions. We conclude which decomposition strategy is likely to provide greater fidelity.

* Thorge.Mueller@dlr.de

II. QAOA

An algorithm of particular interest is the Quantum Approximate Optimization Algorithm (QAOA) [5]. QAOA is a heuristic algorithm aiming to find high-quality solutions to combinatorial optimization problems. It is among the most promising candidates to show quantum supremacy [8] in the near future. A multitude of studies, both numerical [9] and analytical [10, 11], have been performed for QAOA in the ideal zero-error case. Such studies show that while QAOA is universal—any unitary transformation may be expressed in QAOA sequences with driver and problem Hamiltonians—a minimum circuit depth will typically be required to reach the optimal solution of an encoded problem. One important use case of the QAOA algorithm is the approximate solution of MAX-CUT problems, that is, to find low energy states of the problem Hamiltonian

$$H_{\mathrm{P}} = \sum_{(i,j)\in E} Z_i Z_j \,, \tag{1}$$

where E are the edges in a specified problem graph. QAOA consists of layers of alternating Hamiltonians. The

first, the driver Hamiltonian, typically takes the form of single-qubit X rotation gates applied to each qubit. These gates, often described as the transverse field operators in quantum annealing literature[12], are responsible for inducing transitions between computational basis states. and therefore solution states. The QAOA ansatz state is constructed with p pairs of alternating unitaries, determined by the problem and transverse field Hamiltonians,

$$|\boldsymbol{\gamma},\, \boldsymbol{\beta}\rangle_p = U_{\mathrm{M}}(\beta_p)U_{\mathrm{P}}(\gamma_p)\ldots U_{\mathrm{M}}(\beta_1)U_{\mathrm{P}}(\gamma_1)\,|s\rangle\ , \quad (2)$$

where $\boldsymbol{\gamma}, \boldsymbol{\beta}$ are classical parameters to be optimized and

$$U_{\mathrm{M}}(\beta) = \exp\left(-i\beta\sum_i X_i\right), \quad U_{\mathrm{P}}(\gamma) = \exp(-\mathrm{i}\gamma H_P)\,, \quad (3)$$

and $|s\rangle = \mathrm{H}^{\otimes n}\,|0\rangle^{\otimes n}$. While most previous works have not considered the effects of imperfect engineering and interactions with the environment, coherent or otherwise, on the performance of QAOA, some authors have analyzed the effects of depolarizing error models on QAOA performance [13, 14]. No study, however, has considered the influence of errors for different gate decompositions, as is the subject of this work. Two-qubit ZZ-gates encode the problem Hamiltonian of interest and evolve the phase of computational basis states with a dependence on an objective function to be optimized.

III. SOURCES OF NOISE IN QAOA

We have two different types of error sources to distinguish. The first one introduces coherent errors. This error represents coherent unitary over-rotations in the system. The second type of error source causes an unwanted non-unitary evolution of the system and introduces incoherent errors. They are typically due to interactions with an environment. Errors stemming from the single-qubit X rotations are of little interest as such gates are typically executed one or more orders of magnitude faster and more precisely than interacting gates regardless of the platform [4, 15, 16]. As interactions with the environment typically induce noise proportional to the duration of the interaction, such gates result in negligible errors. The ZZ-gate

$$R_{ZZ}(\gamma) = \begin{pmatrix} 1 & 0 & 0 & 0 \\ 0 & e^{i\gamma} & 0 & 0 \\ 0 & 0 & e^{i\gamma} & 0 \\ 0 & 0 & 0 & 1 \end{pmatrix} \quad (4)$$

is the two-qubit gate used in the algorithm and is the focus of our investigation of QAOA under the influence of noise. Two-qubit gates are more error-prone due to their more complicated design than single-qubit gates [3]. Some two-qubit gates are constructed by exploiting direct qubit-qubit interactions. Some utilize intermediate ancillary components as in a tunable coupler design [17], in which one inserts an ancilla qubit leading to additional routes for the environment to interact with the system and potentially greater error. Furthermore, such gates typically increase execution times [18], leading to a higher probability of incoherent errors. Different compiling strategies exist for the ZZ-induced gate depending on which two-qubit gates are natively available on a device, with different groups using different approaches. The Google-developed hardware platform supports a novel *fsim* gate [19], which is an XY-gate with a phase shift on the last diagonal element. Devices manufactured by Rigetti support an extended family of XY-gates [20] using a single calibrated two-qubit gate [20]. The Wallraff group at ETH Zürich provides the parametric CP gate [21], and the IBM platform uses a CNOT gate. We investigate the influence on the performance of coherent over-rotation and depolarizing errors in connection with different compilation platforms. We focus primarily on the decomposition of the ZZ-gate with parametric CP versus fixed-angle CZ gate as these gates require different numbers of two-qubit gates to simulate a ZZ-interaction. While the variable angle CZ gate decomposition needs two fixed CZ gates, the parametric CP gate requires one.

IV. IMPLEMENTATIONS OF THE ZZ-GATE

Depending on the native two-qubit gate in a specific hardware platform, the decomposition of the ZZ-gate takes different forms. In this section, we describe the decompositions into iSWAP, CZ, and CP gates, which are typically available on superconducting devices. In contrast to the CP and CZ, the decomposition into iSWAP is less well-known. First, we investigate $R_{ZZ}(\gamma)$ into CP decomposition

$R_{ZZ}(\gamma) =$ 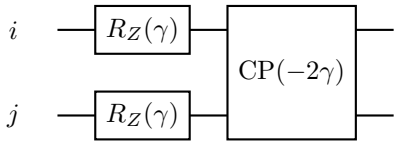

, (5)

$$\text{with} \quad \mathrm{CP}(\gamma) = \begin{pmatrix} 1 & 0 & 0 & 0 \\ 0 & 1 & 0 & 0 \\ 0 & 0 & 1 & 0 \\ 0 & 0 & 0 & e^{i\gamma} \end{pmatrix}. \quad (6)$$

The single-qubit Z-rotation gate $R_Z(\gamma)$ is defined by

$$R_Z(\gamma) = \begin{pmatrix} 1 & 0 \\ 0 & e^{i\gamma} \end{pmatrix}. \quad (7)$$

The circuit diagram of $R_{ZZ}(\gamma)$ in CP decomposition can also be written as $R_{ZZ}(\gamma) = \mathrm{CP}(-2\gamma)R_{Z_1}(\gamma)\,R_{Z_2}(\gamma)$. The Wallraff group introduced this decomposition [21] consisting of two single-qubit Z-rotations depending on the variational parameter γ and the controlled CP gate, which also depends on γ. The parameterized two-qubit

gate could lead to an overhead in the calibration compared to a fixed-parameter two-qubit gate like the CZ. The decomposition into CZ is according to

$R_{ZZ}(\gamma) =$ 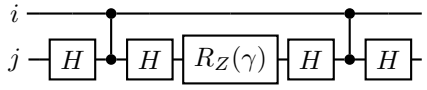 . (8)

The decomposition comprises five single-qubit gates and two fixed two-qubit CZ gates. The rotation angle γ is contained in only one single-qubit Z-rotation. The decomposition into iSWAP requires two two-qubit gates [22] because iSWAP does not belong to the same equivalence class as the ZZ-gate. Furthermore, we demand the iSWAP decomposition to have the following single-qubit rotations: Hadamard and Pauli-Z rotation gate. We further know that the rotation gate containing γ will be sandwiched by the two iSWAP gates. With the help of work concerning XY-based interactions [23] it is straightforward to show that the compilation from a ZZ-gate into iSWAP reads

$R_{ZZ}(\gamma) =$ 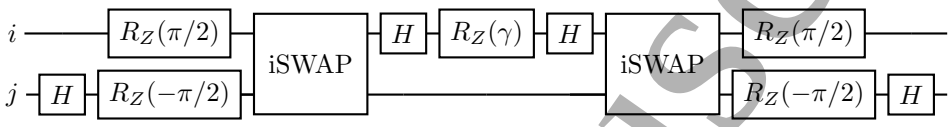 . (9)

The iSWAP gate belongs to the XY family ($XY(\theta = 90)$). Accompanying the two iSWAP gates in the decomposition are 8 single-qubit gates and a Z-rotation which confers the rotation angle γ. Another hardware context in which such gates might be available is that of trapped ion-based quantum computers. These machines natively use a Mølmer–Sørensen gate

$$MS(\gamma) = \exp\left(i\gamma \sum_{l,k} X_l X_k\right) \tag{10}$$

and only need single-qubit rotations to achieve the ZZ-gate [24]. This could also lead to an efficient QAOA compilation. However, this hardware design differs too much from the gate level with superconducting circuits to include it in our comparison. The error sources are also different for these two architectures.

V. DEPOLARIZING AND COHERENT ERRORS IN CP AND CZ

Now we introduce the error channels we apply to our ZZ-gate operations. On the one hand, we want to simulate a coherent error that we incorporate by over-rotation angles θ, ζ in controlled-phase gates $\mathrm{CP}(\theta), \mathrm{CP}(\zeta)$. On the other hand, we apply a two-qubit symmetric depolarizing error channel to our two-qubit gates:

$$\mathcal{E}(\rho) = \frac{pI_4}{4} + (1-p)\rho, \tag{11}$$

with I_4 being the identity matrix for the two-qubit Hilbert space and p the probability that the density matrix ρ will end up in a total mixed state. We assume a Markovian, Pauli-error channel. For simplicity of the simulations, we use the Kraus Operator representation

$$\mathcal{E}(\rho) = \sum_i^{16} m_i K_i \rho K_i^\dagger \quad \text{with} \quad \sum_i^{16} m_i K_i K_i^\dagger = I_4 \tag{12}$$

and $K_i = \omega_{\lfloor \frac{i}{4} \rfloor} \otimes \omega_{i \bmod 4}$ with $\omega = (I_4, X, Y, Z)$. We define $m_1 = \sqrt{1-(15/16)p}$ and otherwise $m_i = \sqrt{p/16}$. X, Y, Z are the Pauli matrices. This is the typically chosen Kraus decomposition for the depolarizing error, which is not unique. We set the incoherent error to a max value of $p = 1\%$ because the gate fidelity declines below 99% for $p > 1\%$. Below 99%, the gate is not suitable for a fault-tolerant quantum computer [25]. The CP gate's coherent error we take into account by adding the error angle θ to $-2\gamma \to -2\gamma + \theta$ leading to the error-prone unitary operation

$$U_{cp}^{co} = R_{Z_2}(\gamma)\, R_{Z_1}(\gamma)\, \mathrm{CP}(-2\gamma + \theta). \tag{13}$$

The coherent error for the CZ gate decomposition we are taken into account by adding a CP with the coherent error phases θ, ζ after the first and the second CZ gate, respectively, leading to the coherent error unitary

$$U_{cz}^{co} = \mathrm{H}_2\, \mathrm{CZ}\, \mathrm{CP}(\theta)\, \mathrm{H}_2 R_{Z_2}(\gamma)\, \mathrm{H}_2\, \mathrm{CZ}\, \mathrm{CP}(\zeta)\, \mathrm{H}_2. \tag{14}$$

The subscripts of U_{cp}^{co} and U_{cz}^{co} describe the gate decomposition and the superscript, the kind of error. For coherent errors, the superscript is *co*, and for decoherent errors *de*. For the error range in the coherent case, we decide to go from 0 to 0.06π ($\approx 3\%$). This is a realistic error range for superconducting platforms. The over-rotation angles θ, ζ are picked independently from a Gaussian function with zero mean and standard deviation $\sigma(\theta)$ or $\sigma(\zeta)$.
The gate fidelity is defined as the average of the integral over all state fidelities

$$F(\rho, \rho') = \left(\mathrm{Tr}\left(\sqrt{\sqrt{\rho}\rho'\sqrt{\rho}}\right)\right)^2. \tag{15}$$

ρ' and ρ are the output density matrices after the gate operation with and without error. Poyatos et al. [26] showed that the integral for the gate fidelities reduces to a sum over 16 initial input states $|\psi_j\rangle = |\psi_a\rangle_1 |\psi_b\rangle_2$ (a,b = 1,..,4; j=1,..,16) with

$$\begin{aligned} &|\psi_1\rangle = |0\rangle, |\psi_2\rangle = |1\rangle, \\ &|\psi_3\rangle = \frac{1}{\sqrt{2}}(i|1\rangle + |0\rangle), |\psi_4\rangle = \frac{1}{\sqrt{2}}(|1\rangle + |0\rangle). \end{aligned} \tag{16}$$

Furthermore, if we consider that the output state after applying the error-free gate operation is always pure, we deduce from eq. (15) the gate fidelity

$$\mathcal{F} = \frac{1}{16}\sum_{j=1}^{16} f_j = \frac{1}{16}\sum_{j=1}^{16} \left\langle \psi_j \right| U^\dagger \rho'_j U \left| \psi_j \right\rangle. \tag{17}$$

ρ'_j is the state ψ_j after applying the decomposition of CZ or CP with the error. In contrast to U, which describes the gate operation without error. f_j is the sate fidelity referred to the state ψ_j.We first apply the error channels separately and then together to analyze the different effects of both errors. The iSWAP decomposition consists of two fixed two-qubit gates like CZ. We are not expecting a different gate fidelity compared to CZ decomposition. CZ and iSWAP decomposition only differs in single-qubit gates, and the error channels do not affect single-qubit gates. Only the state fidelities will change. For this reason, we are not investing in numerical and analytical studies for iSWAP decomposition and refer to CZ decomposition instead.

VI. NUMERICAL STUDIES AND ANALYTICAL RESULTS

In this section, we apply the coherent and incoherent error channels to the ZZ-gate decomposition we have introduced before. We compare how the gate fidelities change. We analyze the gate fidelity for pure coherent over-rotation, see eq. (13) and (14). The quantum fault-tolerance theorem makes no statement about the error threshold specifically for coherent errors but for incoherent errors. The limit for the worst case error is lower in the coherent case due to more efficiency for existing surface codes [27–29]. If we have a pure coherent error U^{co} we have the erroneous density matrix $\rho'_j = U^{co}|\psi_j\rangle\langle\psi_j|(U^{co})^\dagger$ and we can rewrite eq. (17) to

$$\begin{aligned} \mathcal{F}^{co} &= \frac{1}{16}\sum_{j=1}^{16} \langle\psi_j|U^\dagger U^{co}|\psi_j\rangle\langle\psi_j|(U^{co})^\dagger U|\psi_j\rangle \\ \mathcal{F}^{co} &= \frac{1}{16}\sum_{j=1}^{16} |\langle\psi_j|U^\dagger U^{co}|\psi_j\rangle|^2, \end{aligned} \tag{18}$$

with $U^\dagger$ the error-free gate operation and U^{co} the coherent error operation and $\mathcal{F}^{co}$ indicates, that the gate fidelity we are investigating has a coherent error for the erroneous gate operation. If we now decompose into CP gate with $U = R^\dagger_{ZZ}(\gamma)$ and $U^{co} = U^{co}_{cp}$, and inset into eq. (18), we derive the gate fidelity

$$\begin{aligned} \mathcal{F}^{co}_{cp} &= \frac{1}{16}\sum_{j=1}^{16} |\langle\psi_j|R^\dagger_{ZZ}(\gamma)\, U^{co}_{cp}|\psi_j\rangle|^2 \\ &= \frac{1}{16}\sum_{j=1}^{16} |\langle\psi_j| R^\dagger_{Z_1}(\gamma)\, R^\dagger_{Z_2}(\gamma)\, \mathrm{CP}^\dagger(\gamma) \\ &\times R_{Z_1}(\gamma)\, R_{Z_2}\, \mathrm{CP}(\gamma+\theta)\,|\psi_j\rangle|^2 \\ &= \frac{1}{16}\sum_{j=1}^{16} |\langle\psi_j|\mathrm{CP}(\theta)|\psi_j\rangle|^2. \end{aligned} \tag{19}$$

The gate fidelity $\mathcal{F}^{co}_{cp}$ is independent of the rotation angle γ. This is because the error $\mathrm{CP}(\theta)$ as well as the error-free gate Operation U_{cp} are diagonal. The gate operations can thus commute through and cancel out. We can now calculate the 16 state fidelities. We achieve the following state fidelities f_j equations for all 16 input states:

$$\begin{aligned} f_{1,2,3,6,7,10,11,16} &= 1, \\ f_{12,13,14,15} &= \frac{(2+2\cos(\theta))}{4}, \\ f_{4,5,8,9} &= \frac{(10+6\cos(\theta))}{16}. \end{aligned} \tag{20}$$

By inserting all state fidelities of eq. (20), we simplify eq. (19) to

$$\begin{aligned} \mathcal{F}^{co}_{cp} &= \frac{1}{16}\sum_{j=1}^{16} |\langle\psi_j|\mathrm{CP}(\theta)|\psi_j\rangle|^2 \\ &= \frac{1}{2} + \frac{1}{4}\frac{(2+2\cos(\theta))}{4} + \frac{1}{4}\frac{(10+6\cos(\theta))}{16} \\ &= \frac{1}{32}(25+7\cos(\theta)). \end{aligned} \tag{21}$$

Figure 1 presents the results for the gate fidelity (Eq. (21)) and the corresponding state fidelities (Eq. (20)). The plot shows the fidelities as a function of the standard deviation $\sigma(\theta)$, with the Gaussian error fixed at 3%. The different contributions of the state fidelities to the gate fidelity in the CP decomposition, $\mathcal{F}^{co}_{cp}$, are shown. It should be noted that the constant state fidelities described by Eq. (20) are not explicitly shown in the plot. For a high coherent error of approximately 3%, the gate fidelity is around 99.6%. The decomposition into CZ gates is not diagonal, and therefore, the error channel $\mathrm{CP}(\theta)$ cannot commute through and cancel out. If we insert the error-free and erroneous gate operation, see eq. (14), for

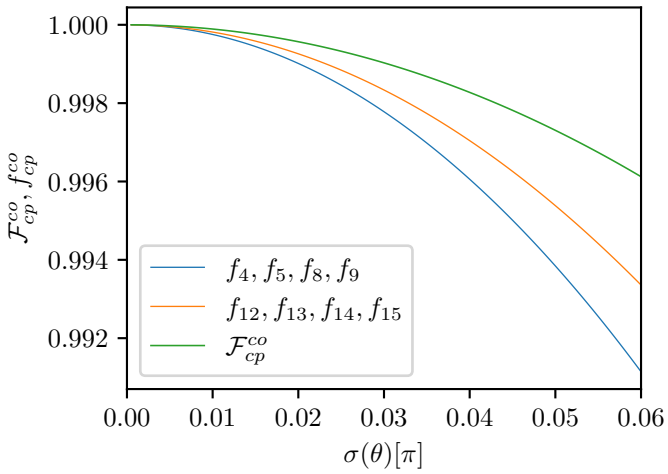

FIG. 1: Gate $\mathcal{F}_{cp}^{co}$ and state f_j^{co} fidelities (y-axis) plotted against the standard deviation $\sigma(\theta)$ for the Gaussian coherent error (x-axis) for CP decomposition. The graph shows the gate fidelity and the split into 16 state fidelities. The solid green line represents the gate fidelity $\mathcal{F}_{cp}^{co}$, and the orange and the blue line represent the state fidelities. The error-unaffected state fidelities are not shown.

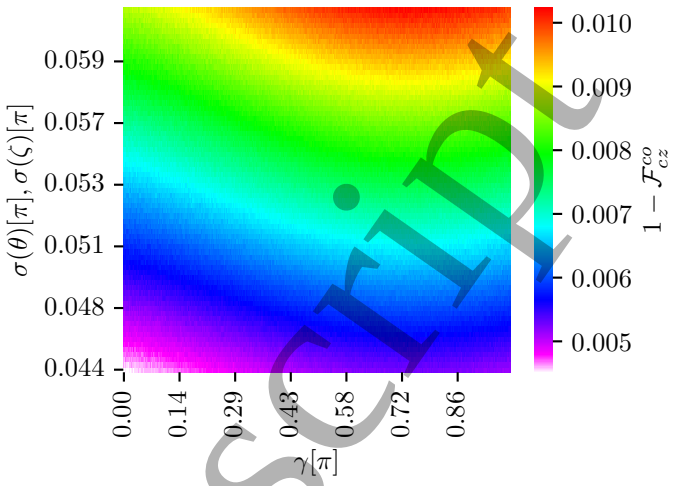

FIG. 2: Gate infidelity 1-$\mathcal{F}_{cz}^{co}$ (colorbar) for the Gaussian coherent error with standard deviations $\sigma(\theta), \sigma(\zeta)$ (y-axis) and the rotation angle γ (x-axis). The colorbar indicates the infidelity: a low value in the red regime(top-right) corresponds to a low fidelity of 99 %. The magenta regime's high value(bottom-left) relates to a high gate fidelity of 99.5 %. We average over 1000 repetitions per angle and error.

the CZ decomposition into eq. (18) we derive

$$\begin{aligned}\mathcal{F}_{cz}^{co} &= \frac{1}{16}\sum_{j=1}^{16} |\langle\psi_j|(R_{ZZ}^{\dagger}(\gamma)U_{cz}|\psi_j\rangle|^2 \\ &= \frac{1}{16}\sum_{j=1}^{16} |\langle\psi_j|(R_{ZZ}^{\dagger}(\gamma)\,\mathrm{H}_2\,\mathrm{CZ}\,R_{X_2}(\gamma)\,\mathrm{CZ}\,\mathrm{H}_2|\psi_j\rangle|^2.\end{aligned} \tag{22}$$

The closed solution for the gate fidelity $\mathcal{F}_{cz}^{co}$ exceeds the space constraint. Therefore, we assume small angles θ, ζ. For the gate fidelity of CZ, we calculate the 16 state fidelities up to the second order in θ, ζ. If we sum up all state fidelities and make the small angle approximation for ζ and θ, we derive the following equation for the coherent error in CZ decomposition

$$\begin{aligned}\mathcal{F}_{cz}^{co} &= \frac{1}{16}\sum_{j=1}^{16} |\langle\psi_j|U_{cz}^{\dagger}U_{cz}^{co}|\psi_j\rangle|^2 \\ &= 1 - 0.12\,\theta^2 - 0.13\,\zeta^2 - 0.05\,\theta\zeta \\ &- 0.02\,\theta\zeta\sin(\gamma) - 0.19\,\theta\zeta\cos(\gamma) - 0.02\,\zeta^2\sin(\gamma) \\ &+ 0.02\,\zeta^2\cos(\gamma) + \mathcal{O}(h),\end{aligned} \tag{23}$$

with h being all terms depending on ζ, θ up to order three. In contrast to $\mathcal{F}_{cp}^{co}$, $\mathcal{F}_{cz}^{co}$ shows a weak dependency on the rotation angle γ. Thus $\mathcal{F}_{cz}^{co}$ consists of small coherent over-rotation angles θ, ζ coupled to γ with $\sin(\gamma)\theta$ and $\cos(\gamma)\theta$. The numerical results for the CZ decomposition are shown in fig. 2. In fact, for small $\sigma(\zeta), \sigma(\theta) < 0.04\pi$, the dependency on γ is weaker, and we recover the quadratic law from small error approximation of the cosine like for the CP decomposition.

The minimum of the gate fidelity is at $\gamma = 0.72\pi$ depending on $\sigma(\zeta), \sigma(\theta)$. For example, at this minimum, we attain a gate infidelity of 0.75 % at a standard deviation $\sim \sigma(\zeta), \sigma(\theta) = 0.054\pi$ (2.7 %). The same infidelity we derive at $\gamma = 0$ at a standard deviation $\sigma(\zeta), \sigma(\theta) = 0.0585\pi$ (2.9 %). Conversely, if we fix $\zeta(\zeta), \sigma(\theta) = 0.056\pi$, the gate infidelity is approximately 0.7 % at a rotation angle of zero. The infidelity is 0.85 % for the same standard deviation at the minimum of $\gamma = 0.72\pi$. Consequently, the small rotations angles $\gamma \approx 0$ and the larger ones $\gamma \approx \pi$ are more error robust against coherent noise than close to $\gamma \approx 0.72\pi$. The gate fidelity difference in dependence of γ is negligible for $\zeta(\zeta), \sigma(\theta) < 0.04\pi$. The gate fidelity threshold of 99 % is reached for a standard deviation $\sigma(\zeta), \sigma(\theta) > 0.06\pi$. Further, we can simplify eq. (23) to

$$\mathcal{F}_{cz}^{co} = 1 - \theta^2(0.3 + 0.04\sin(\gamma) + 0.17\cos(\gamma)) + \mathcal{O}(\theta^3), \tag{24}$$

if we assume $\zeta = \theta$. We can use this equation for potential extreme errors in one single ZZ-gate where both CZ gates face the highest possible error from the Gaussian error distribution. Fig. 3 allows us to estimate the gate infidelity for high and low standard deviations $\sigma(\theta)$ depending on the rotation angle γ. As we increase the standard deviation $\sigma(\theta)$, the variation in the gate fidelity through the rotation angle γ increases.We plotted here the analytic function and not averaging over a randomly picked Gaussian distribution for $\sigma(\theta)$ as in fig. 2. In this case, we see a shift in the numerical results in fig. 2. Here we see the opposite side; gate fidelities are higher for small rotation angles γ than for high rotation angles.

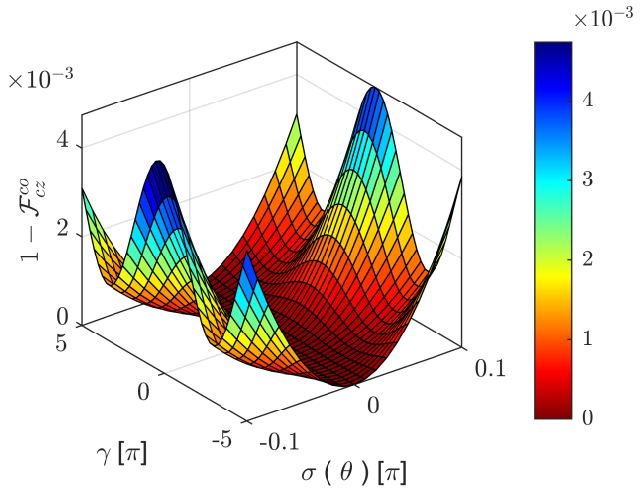

FIG. 3: plot of eq. (24) for a standard deviation $\sigma(\theta) \in [-0.1\pi, 0.1\pi]$ and $\gamma \in [-1.5\pi, 1.5\pi]$.

But the overall trend in fig. 3 is the same as for fig 2. We now turn to the case of a pure depolarizing error for CP,

$$F_{cp}^{de} = \frac{1}{16}\sum_{j=1}^{16} \langle\psi_j| U^{cp\dagger}\mathcal{E}(U^{cp}|\psi_j\rangle\langle\psi_j| U^{cp\dagger})U^{cp}|\psi_j\rangle\,, \tag{25}$$

and for CZ decomposition,

$$F_{cz}^{de} = \frac{1}{16}\sum_{j=1}^{16} \langle\psi_j| U^{cz\dagger}\mathcal{E}(\mathcal{E}(U^{cz}|\psi_j\rangle\langle\psi_j| U^{cz\dagger}))U^{cz}|\psi_j\rangle\,. \tag{26}$$

Fig. 4 shows the gate fidelity behaviour under the depolarizing error for CP and CZ, $\mathcal{F}_{cp}^{de}$ and $\mathcal{F}_{cz}^{de}$, respectively. To accomplish a fully error-corrected quantum computer, the available two-qubit gate's fidelity must be well above

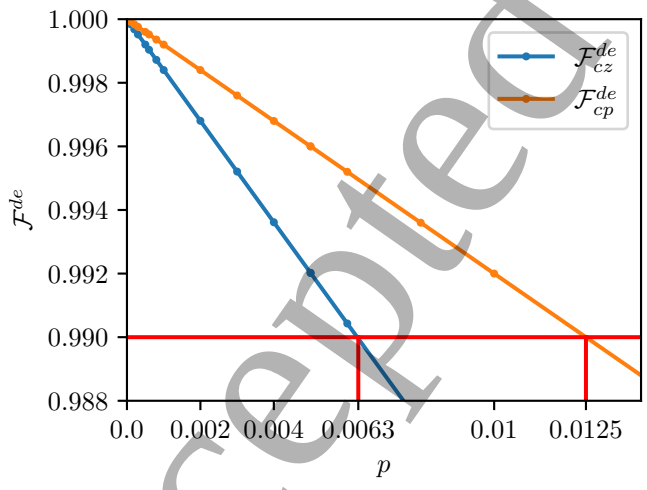

FIG. 4: Gate fidelities plotted against depolarizing error for CP (orange) and CZ (blue) decomposition. The red line indicates the 99 % gate fidelity.

the limit of 99 % [25, 30]. The exact threshold value is an ongoing discussion. For specific connectivity graphs, this threshold could also be lower than 99% [31]. $\mathcal{F}_{cz}^{de}$ drops below 99% gate fidelity for $p > 0.63$ %. In contrast $\mathcal{F}_{cp}^{de}$ is more error robust. The threshold value of 99 % is reached for $p = 1.25$ %. The linear behavior of $\mathcal{F}_{cp}^{de} = 1 - 0.8p$ follows directly from the definition of the symmetric two-qubit depolarizing error channel. There is no dependency on the rotation angle γ. The gate fidelity for $\mathcal{F}_{cp}^{de} = 1 - 1.54p$ is deduced by applying the error channel twice. After utilizing the channel a second time to the density matrix, the equation $\mathcal{F}_{cz}^{de} = 1 - (3/2)p + (3/4)p^2$ is derived. For small error p, the linear scaling will be achieved. By applying the incoherent error channel twice, the limit for depolarizing error before crossing the 99 % line is approximately doubled. In both cases, the single-state fidelities for all 16 states are equal.
Next, we apply both error models simultaneously to both ZZ-gate decompositions. Fig. 5 shows the difference

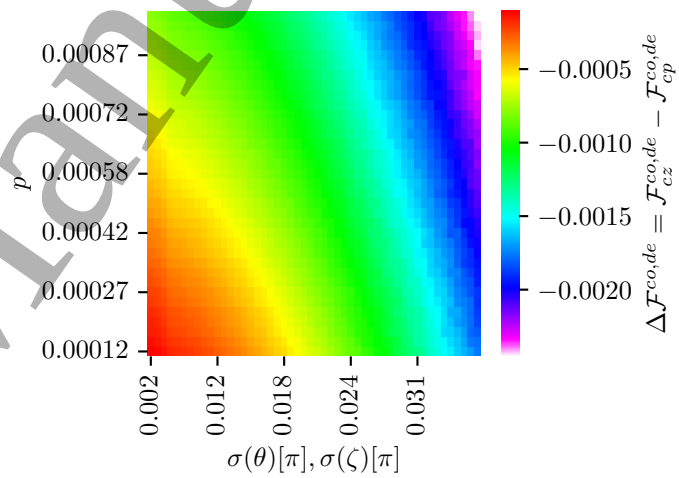

FIG. 5: Plotting the fidelity difference $\mathcal{F}_{cp} - \mathcal{F}_{cz}$ in dependency on the coherent error's standard deviations $\sigma(\zeta), \sigma(\theta)$ (x-axis) and the depolarizing error P (y-axis). magenta corresponds to a high advantage of F_{cp} over F_{cz} whereas red correspond to comparable gate fidelity of both decompositions.

in gate fidelities $\Delta\mathcal{F}^{de,co}$ between $\mathcal{F}_{cp}^{de,co}$,$\mathcal{F}_{cz}^{de,co}$ for coherent and depolarizing error. For fig. 5, we set the rotation angle to a small value of $\gamma = 0.01\pi$ to achieve the greatest F_{cz}^{co}. The plot shows gate fidelities above 99 %. If $\sigma(\zeta), \sigma(\theta) < 0.016$ (0.8 %) and $p < 0.032\%$ the difference in the fidelities between both decompositions is $\Delta\mathcal{F}^{de,co} \approx 0.02\%$. For standard deviations $\sigma(\zeta), \sigma(\theta) < 0.016$ (0.8 %), $p < 0.032\%$ gate fidelities are of order $\mathcal{F}_{cz}^{de,co}, \mathcal{F}_{cp}^{de,co} \approx 99.8$ %. As a result, if we could suppress the incoherent error and allow for small coherent over-rotations, there is no advantage from CP over CZ decomposition. Of course, the circuit depth would double in the case of the CZ decomposition technique and could exceed coherence time. On the other hand, the pulse calibration for different angles for the parametric CP gate

would also lead to another error source. As hardware platforms achieve small standard deviations for the Gaussian error model of $\sigma(\zeta), \sigma(\theta) < 0.016\pi$, and small depolarizing error $p < 0.032\%$, we can compare both schemes on a device. If the depolarizing error and the coherent error increase, we achieve a fidelity difference $\Delta\mathcal{F}^{de,co} \approx 0.3\%$ (fig. 5; purple region). In fig. 5, $\mathcal{F}_{cp}^{co,de} \approx 99.8\%$ for the whole error range, whereas $\mathcal{F}_{cz}^{co,de}$ declines to 99.5% (top-right corner in fig. 5) for large error rates. Therefore, the advantage of having a CP decomposition over CZ for large error rates is numerically proven. By increasing the incoherent error $p > 0.1\%$, the dominance of the linear scaling law of the depolarizing error over the squared scaling of the coherent error would be identified. Thus the heatmap would change from a radial trend caused by the influence of $\sigma(\zeta), \sigma(\theta)$ and p on the gate fidelities to a linear scaling in p direction(y-axis).

VII. INCOHERENT ERROR SOURCES: DISCUSSING LEAKAGE AND CROSSTALK

In this section, we examine the current state of the art on crosstalk and leakage errors, and the extent to which they contribute to the overall error budget from the previous section.

Our model demonstrates the limitations and conditions under which the CZ and CP gates perform similarly and deliver comparable results for QAOA. Previous studies have extensively investigated leakage errors, which are included in our error budget for incoherent errors. Specifically, for the CZ gate in superconducting transmon qubits, Rol et al. [32] introduced a scheme that suppresses leakage error to 0.1 %, achieving an average gate fidelity of 99.1 %. Additionally, Miao et al. [33] showed that by implementing a surface code on Google's Sycamore chip, they reduced the leakage error from 1 % to 0.1 %. These schemes provide realistic estimates for leakage error, supporting our acceptance of a 0.1 % leakage error in the incoherent error budget. While the CP gate has not been specifically analyzed for leakage, its calibration is not significantly different from the CZ gate. Therefore, we assume the same leakage error for CP based on the same architectures with a different calibration. For one-qubit gates (which are not subject to analysis), current schemes, such as the DRAG pulse, can reduce leakage errors to as low as 0.044 %, as demonstrated by Werninghaus et al. [34].

Crosstalk is another source of incoherent noise that we consider in our error budget estimation. We do not explicitly simulate its effect, as it requires an analysis that encompasses more than a single two-qubit gate. To address this, we either need to analyze a real experiment or simulate the entire topology of a quantum device. Nonetheless, this analysis has been conducted. Arute et al. [35], in their renowned supremacy experiment, demonstrated how to handle crosstalk on a real device. They showed that for CZ gates on the Sycamore chip, the fidelity of an isolated two-qubit gate achieved 0.36 % infidelity. When measuring the fidelity of all entangled two-qubit gates simultaneously, the infidelity was 0.62 %. This indicates that crosstalk does not significantly affect the gate infidelity on transmon qubits by orders of magnitude. Furthermore, in 2022, Winick et al. [36] proposed a scheme to optimize control pulses for a square lattice of 100 transmon qubits for CNOT gates, theoretically reducing the crosstalk error by 1-2 orders of magnitude, making it negligible. Since the topology remains unchanged for CP gates, we expect similar results for them as well as for CZ gates, for small-sized devices with approximately 10-20 qubits. In general, both the experimental study and the theoretical scheme suggest that in our error budget for incoherent errors, crosstalk can be disregarded or, at the very least, does not increase the error rate significantly.

When considering the scaling of larger qubit systems, the situation changes. The CP gate often requires fine-tuned, dynamic parameter control to implement different phase shifts. This can lead to higher calibration overhead, especially when maintaining high fidelity in large-scale systems. Calibrating CP gates on devices with many qubits becomes more complex because each phase shift must be precisely controlled, resulting in more complicated parameter tuning. Furthermore, as larger devices incorporate more qubits and control channels within a compact space, sensitivity to crosstalk increases, reducing fidelity due to unintended interactions between qubits. In contrast, the CZ gate applies a fixed phase shift of π, making it a simpler, fixed-phase gate with lower calibration complexity compared to the CP gate. CZ gates are typically easier to calibrate, as they require fewer dynamic parameters and often use less time-varying control (e.g., fixed duration and amplitude). Consequently, CZ gates can achieve higher fidelities in large-scale devices because their simpler design reduces the calibration overhead across the system. Thus, in large-scale quantum processors, architectures based on CZ gates are less prone to crosstalk than those based on CP gates.

VIII. COMPARRSION TO EXPERIMENTAL DATA

To compare our results with real experimental data, we can use the best available current data. For the CZ gate, we use the 72-qubit Sycamore chip from Google Quantum AI [37], which achieves a fidelity of about 99.4 %. Evered et al. [38] report a similar gate fidelity of 99.5 % for CZ gates on a neutral atom quantum device, rather than superconducting hardware. Additionally, we could calibrate both the Sycamore chip and the neutral atom hardware to achieve the same gate fidelity for the CP gate. Building on Levine et al.'s [39] experiment, Pagano et al. [40] theoretically showed that a CP gate fidelity of 99.9 % can be achieved with Rydberg atoms. Despite these advancements, these two-qubit gate fidelities are significantly lower than what we require for our study.

We compare gate fidelities of the order of 99.99 % in the previous sections. Therefore, to run a real experiment and obtain comparable results for QAOA, the current gate fidelities are insufficient. They are too low to make a meaningful comparison for a circuit and to accurately distinguish between the influences of coherent and incoherent noise, given the dominance of incoherent noise at present.

IX. ERROR REDUCTION OF TWO-QUBIT GATES

In this section, we provide an overview from various perspectives on potential approaches to managing errors in supercondcuting quantum devices.

Quantum error correction: In advancing our quantum device, we aim to implement quantum error correction techniques. The CNOT gate belongs to the Clifford+T group, which can be utilized as a universal gate set. Stabilizer codes, needed for qubit error correction, have a natural representation within the Clifford group. However, implementing non-Clifford gates requires the use of magic state distillation [41], a process that is both complex and resource-intensive [42]. The CP gate is a non-Clifford gate, and its incorporation introduces a significant overhead in the implementation of fault-tolerant quantum computing, compared to the CZ gate, which, like the CNOT gate, belongs to the same equivalence class within the Clifford group. CZ gate could therefore lead to a less error-prone fault-tolerant hardware implementation.

Pulse shaping: For the CZ gate, we assume the system operates at the quantum speed limit (QSL), implying the gate time is effectively zero. The CP gates, operating at various phase angles θ and collectively known as the CP(θ) family, typically correspond to different gate times, with shorter gate times reducing the qubits' exposure to decoherence but potentially introducing higher-frequency noise due to rapid control changes. CP gates are particularly sensitive to the high-frequency components of control signals [43], which can lead to effects such as leakage or crosstalk. To mitigate these errors, using smooth pulse shapes—such as Gaussian or DRAG pulses—rather than square pulses, helps to minimize high-frequency components in the pulse spectrum, thereby reducing leakage. Thus, an effective pulse-shaping strategy for CP gates involves optimizing the pulse to minimize errors while maintaining a reasonable gate time. For example, slightly stretching a Gaussian pulse can reduce high-frequency noise without extending the gate time beyond the qubit's coherence time. So we can make the whole CP(θ) family more error robust by adjusting the pulse shapes. We recommend the strategies of Rimbach-Rus et al. [44].

Post-selection methods: One potential strategy for error mitigation is the use of post-selection methods. However, we advise against employing these techniques for superconducting qubits, where CZ and CP gates are natively available. Post-selection methods typically involve the use of ancillary qubits to enhance error detection and flagging. By entangling these ancillary qubits with the computational qubits, one can effectively monitor for errors during computation, facilitating the decision to discard specific outcomes during the post-selection process. While superconducting systems can incorporate ancillary qubits, their short coherence times limit the efficacy of this approach compared to ion trap-based quantum computers for instance.

Composite pulse sequences: In our studies, we assume the application of established techniques, specifically composite pulse sequences, to enhance gate fidelities by mitigating various sources of error. We recommend employing the approach developed by Calderón-Vargas et al. [45] to effectively reduce coherent systematic logical errors, such as those arising from low-frequency noise and the over- and under-rotation of qubits. The BB1 variant for two-qubit gates is particularly advantageous for improving coherent overrotations.

X. CONCLUSION

We showed that the decomposition of the ZZ-gate into CP gate achieves greater gate fidelities compared to the CZ-gate decomposition in both incoherent and coherent error channels. By suppressing the depolarizing error below 0.03 % and having a coherent error in the range of 1%, both gate decompositions deliver comparable fidelities and could be used especially in the case of variational algorithms. The variational algorithm could deal with the coherent error due to the optimization process. For a coherent over-rotation $\theta > 0.04\pi$, the gate fidelity in the CZ decomposition depends on the rotation angle γ. For $\zeta(\theta), \sigma(\theta) = 0.054\pi$, the gate fidelity differs by 0.1%, which is significant concerning the quantum threshold theorem where a difference around 0.1% could make a difference of 1000 physical qubits per logical qubit [25]. A fixed two-qubit gate like CZ in combination with single-qubit gates designed by virtual Z gates could lead to a significant calibration reduction and less errors on pulse level. When the coherent over-rotation angle is below $\theta < 0.016\pi$ (0.8 %) and the incoherent error is suppressed below 0.03 %, we recommend CZ with virtual Z gates. To execute QAOA effectively, we recommend using the CZ decomposition for a short circuit depth and low incoherent error below $p \leq 0.03\%$. Additionally, based on Marshall et al. [46], we anticipate that deviations in the expectation value of QAOA will remain below 1 %.

ACKNOWLEDGMENTS

The authors acknowledge funding, support, and computational resources from German Aerospace Center (DLR) and the Forschungszentrum Jülich. Furthermore, we acknowledge funding from QSolid funded by the Federal Ministry of Education and Research (BMBF). We also

acknowledge funding from AQUAS and QUASIM, both funded by the Federal Ministry of Economic Affairs and Climate Action (BMWK). We acknowledge useful conversations with Alessandro Ciani and Tim Bode.

[1] P. W. Shor, Polynomial-time algorithms for prime factorization and discrete logarithms on a quantum computer, SIAM J. Comput. **26**, 1484–1509 (1997).

[2] L. K. Grover, A fast quantum mechanical algorithm for database search, in *Proceedings of the Twenty-Eighth Annual ACM Symposium on Theory of Computing* (Association for Computing Machinery, New York, NY, USA, 1996) p. 212–219.

[3] F. Arute, K. Arya, R. Babbush, D. Bacon, J. C. Bardin, R. Barends, R. Biswas, S. Boixo, F. G. S. L. Brandao, D. A. Buell, B. Burkett, Y. Chen, Z. Chen, B. Chiaro, R. Collins, W. Courtney, A. Dunsworth, E. Farhi, B. Foxen, A. Fowler, C. Gidney, M. Giustina, R. Graff, K. Guerin, S. Habegger, M. P. Harrigan, M. J. Hartmann, A. Ho, M. Hoffmann, T. Huang, T. S. Humble, S. V. Isakov, E. Jeffrey, Z. Jiang, D. Kafri, K. Kechedzhi, J. Kelly, P. V. Klimov, S. Knysh, A. Korotkov, F. Kostritsa, D. Landhuis, M. Lindmark, E. Lucero, D. Lyakh, S. Mandrà, J. R. McClean, M. McEwen, A. Megrant, X. Mi, K. Michielsen, M. Mohseni, J. Mutus, O. Naaman, M. Neeley, C. Neill, M. Y. Niu, E. Ostby, A. Petukhov, J. C. Platt, C. Quintana, E. G. Rieffel, P. Roushan, N. C. Rubin, D. Sank, K. J. Satzinger, V. Smelyanskiy, K. J. Sung, M. D. Trevithick, A. Vainsencher, B. Villalonga, T. White, Z. J. Yao, P. Yeh, A. Zalcman, H. Neven, and J. M. Martinis, Quantum supremacy using a programmable superconducting processor, Nature **574**, 505 (2019).

[4] R. Barends, J. Kelly, A. Megrant, A. Veitia, D. Sank, E. Jeffrey, T. C. White, J. Mutus, A. G. Fowler, B. Campbell, Y. Chen, Z. Chen, B. Chiaro, A. Dunsworth, C. Neill, P. O'Malley, P. Roushan, A. Vainsencher, J. Wenner, A. N. Korotkov, A. N. Cleland, and J. M. Martinis, Superconducting quantum circuits at the surface code threshold for fault tolerance, Nature **508**, 500 (2014).

[5] E. Farhi, J. Goldstone, and S. Gutmann, A quantum approximate optimization algorithm (2014), arXiv:1411.4028 [quant-ph].

[6] A. Peruzzo, J. McClean, P. Shadbolt, M.-H. Yung, X.-Q. Zhou, P. J. Love, A. Aspuru-Guzik, and J. L. O'Brien, A variational eigenvalue solver on a photonic quantum processor, Nature Communications **5**, 4213 (2014).

[7] Y. Suzuki, S. Endo, K. Fujii, and Y. Tokunaga, Quantum error mitigation as a universal error reduction technique: Applications from the nisq to the fault-tolerant quantum computing eras, PRX Quantum **3**, 010345 (2022).

[8] E. Farhi and A. W. Harrow, Quantum supremacy through the quantum approximate optimization algorithm (2019), arXiv:1602.07674 [quant-ph].

[9] L. Zhou, S.-T. Wang, S. Choi, H. Pichler, and M. D. Lukin, Quantum approximate optimization algorithm: Performance, mechanism, and implementation on near-term devices, Phys. Rev. X **10**, 021067 (2020).

[10] M. Streif and M. Leib, Training the quantum approximate optimization algorithm without access to a quantum processing unit, Quantum Science and Technology **5**, 034008 (2020).

[11] V. Akshay, H. Philathong, M. E. S. Morales, and J. D. Biamonte, Reachability deficits in quantum approximate optimization, Phys. Rev. Lett. **124**, 090504 (2020).

[12] M. H. S. Amin, Consistency of the adiabatic theorem, Phys. Rev. Lett. **102**, 220401 (2009).

[13] M. Streif, M. Leib, F. Wudarski, E. Rieffel, and Z. Wang, Quantum algorithms with local particle number conservation: noise effects and error correction (2020), arXiv:2011.06873 [quant-ph].

[14] J. Marshall, F. Wudarski, S. Hadfield, and T. Hogg, Characterizing local noise in QAOA circuits, IOP SciNotes **1**, 025208 (2020).

[15] Y.-C. Yang, S. N. Coppersmith, and M. Friesen, Achieving high-fidelity single-qubit gates in a strongly driven charge qubit with 1/f charge noise, npj Quantum Information **5**, 12 (2019).

[16] G. Tosi, F. A. Mohiyaddin, V. Schmitt, S. Tenberg, R. Rahman, G. Klimeck, and A. Morello, Silicon quantum processor with robust long-distance qubit couplings, Nature Communications **8**, 450 (2017).

[17] X. Li, T. Cai, H. Yan, Z. Wang, X. Pan, Y. Ma, W. Cai, J. Han, Z. Hua, X. Han, Y. Wu, H. Zhang, H. Wang, Y. Song, L. Duan, and L. Sun, Tunable coupler for realizing a controlled-phase gate with dynamically decoupled regime in a superconducting circuit, Phys. Rev. Applied **14**, 024070 (2020).

[18] N. M. Linke, D. Maslov, M. Roetteler, S. Debnath, C. Figgatt, K. A. Landsman, K. Wright, and C. Monroe, Experimental comparison of two quantum computing architectures, Proceedings of the National Academy of Sciences **114**, 3305 (2017).

[19] B. Foxen, C. Neill, A. Dunsworth, P. Roushan, B. Chiaro, A. Megrant, J. Kelly, Z. Chen, K. Satzinger, R. Barends, F. Arute, K. Arya, R. Babbush, D. Bacon, J. C. Bardin, S. Boixo, D. Buell, B. Burkett, Y. Chen, R. Collins, E. Farhi, A. Fowler, C. Gidney, M. Giustina, R. Graff, M. Harrigan, T. Huang, S. V. Isakov, E. Jeffrey, Z. Jiang, D. Kafri, K. Kechedzhi, P. Klimov, A. Korotkov, F. Kostritsa, D. Landhuis, E. Lucero, J. McClean, M. McEwen, X. Mi, M. Mohseni, J. Y. Mutus, O. Naaman, M. Neeley, M. Niu, A. Petukhov, C. Quintana, N. Rubin, D. Sank, V. Smelyanskiy, A. Vainsencher, T. C. White, Z. Yao, P. Yeh, A. Zalcman, H. Neven, and J. M. Martinis (Google AI Quantum), Demonstrating a continuous set of two-qubit gates for near-term quantum algorithms, Phys. Rev. Lett. **125**, 120504 (2020).

[20] D. M. Abrams, N. Didier, B. R. Johnson, M. P. d. Silva, and C. A. Ryan, Implementation of xy entangling gates with a single calibrated pulse, Nature Electronics **3**, 744 (2020).

[21] N. Lacroix, C. Hellings, C. K. Andersen, A. Di Paolo, A. Remm, S. Lazar, S. Krinner, G. J. Norris, M. Gabureac, J. Heinsoo, A. Blais, C. Eichler, and A. Wallraff, Improving the performance of deep quantum optimization algorithms with continuous gate sets, PRX Quantum **1**, 110304 (2020).

[22] E. C. Peterson, G. E. Crooks, and R. S. Smith, Fixed-Depth Two-Qubit Circuits and the Monodromy Polytope, Quantum **4**, 247 (2020).
[23] N. Schuch and J. Siewert, Natural two-qubit gate for quantum computation using the XY interaction, Phys. Rev. A **67**, 032301 (2003).
[24] I. Cohen, S. Weidt, W. K. Hensinger, and A. Retzker, Multi-qubit gate with trapped ions for microwave and laser-based implementation, New Journal of Physics **17**, 043008 (2015).
[25] D. S. Wang, A. G. Fowler, and L. C. L. Hollenberg, Surface code quantum computing with error rates over 1 %, Phys. Rev. A **83**, 020302 (2011).
[26] J. F. Poyatos, J. I. Cirac, and P. Zoller, Complete characterization of a quantum process: The two-bit quantum gate, Phys. Rev. Lett. **78**, 390 (1997).
[27] S. Bravyi, M. Englbrecht, R. König, and N. Peard, Correcting coherent errors with surface codes, npj Quantum Information **4**, 55 (2018).
[28] J. Wallman, C. Granade, R. Harper, and S. T. Flammia, Estimating the coherence of noise, New Journal of Physics **17**, 113020 (2015).
[29] E. Huang, A. C. Doherty, and S. Flammia, Performance of quantum error correction with coherent errors, Phys. Rev. A **99**, 022313 (2019).
[30] A. G. Fowler, A. M. Stephens, and P. Groszkowski, High-threshold universal quantum computation on the surface code, Phys. Rev. A **80**, 052312 (2009).
[31] A. G. Fowler, M. Mariantoni, J. M. Martinis, and A. N. Cleland, Surface codes: Towards practical large-scale quantum computation, Phys. Rev. A **86**, 032324 (2012).
[32] M. A. Rol, F. Battistel, F. K. Malinowski, C. C. Bultink, B. M. Tarasinski, R. Vollmer, N. Haider, N. Muthusubramanian, A. Bruno, B. M. Terhal, and L. DiCarlo, Fast, high-fidelity conditional-phase gate exploiting leakage interference in weakly anharmonic superconducting qubits, Phys. Rev. Lett. **123**, 120502 (2019).
[33] K. C. Miao, M. McEwen, J. Atalaya, D. Kafri, L. P. Pryadko, A. Bengtsson, A. Opremcak, K. J. Satzinger, Z. Chen, P. V. Klimov, C. Quintana, R. Acharya, K. Anderson, M. Ansmann, F. Arute, K. Arya, A. Asfaw, J. C. Bardin, A. Bourassa, J. Bovaird, L. Brill, B. B. Buckley, D. A. Buell, T. Burger, B. Burkett, N. Bushnell, J. Campero, B. Chiaro, R. Collins, P. Conner, A. L. Crook, B. Curtin, D. M. Debroy, S. Demura, A. Dunsworth, C. Erickson, R. Fatemi, V. S. Ferreira, L. F. Burgos, E. Forati, A. G. Fowler, B. Foxen, G. Garcia, W. Giang, C. Gidney, M. Giustina, R. Gosula, A. G. Dau, J. A. Gross, M. C. Hamilton, S. D. Harrington, P. Heu, J. Hilton, M. R. Hoffmann, S. Hong, T. Huang, A. Huff, J. Iveland, E. Jeffrey, Z. Jiang, C. Jones, J. Kelly, S. Kim, F. Kostritsa, J. M. Kreikebaum, D. Landhuis, P. Laptev, L. Laws, K. Lee, B. J. Lester, A. T. Lill, W. Liu, A. Locharla, E. Lucero, S. Martin, A. Megrant, X. Mi, S. Montazeri, A. Morvan, O. Naaman, M. Neeley, C. Neill, A. Nersisyan, M. Newman, J. H. Ng, A. Nguyen, M. Nguyen, R. Potter, C. Rocque, P. Roushan, K. Sankaragomathi, H. F. Schurkus, C. Schuster, M. J. Shearn, A. Shorter, N. Shutty, V. Shvarts, J. Skruzny, W. C. Smith, G. Sterling, M. Szalay, D. Thor, A. Torres, T. White, B. W. K. Woo, Z. J. Yao, P. Yeh, J. Yoo, G. Young, A. Zalcman, N. Zhu, N. Zobrist, H. Neven, V. Smelyanskiy, A. Petukhov, A. N. Korotkov, D. Sank, and Y. Chen, Overcoming leakage in quantum error correction, Nature Physics **19**, 1780 (2023).
[34] M. Werninghaus, D. J. Egger, F. Roy, S. Machnes, F. K. Wilhelm, and S. Filipp, Leakage reduction in fast superconducting qubit gates via optimal control, npj Quantum Information **7**, 14 (2021).
[35] F. Arute, K. Arya, R. Babbush, D. Bacon, J. C. Bardin, R. Barends, R. Biswas, S. Boixo, F. G. S. L. Brandao, D. A. Buell, B. Burkett, Y. Chen, Z. Chen, B. Chiaro, R. Collins, W. Courtney, A. Dunsworth, E. Farhi, B. Foxen, A. Fowler, C. Gidney, M. Giustina, R. Graff, K. Guerin, S. Habegger, M. P. Harrigan, M. J. Hartmann, A. Ho, M. Hoffmann, T. Huang, T. S. Humble, S. V. Isakov, E. Jeffrey, Z. Jiang, D. Kafri, K. Kechedzhi, J. Kelly, P. V. Klimov, S. Knysh, A. Korotkov, F. Kostritsa, D. Landhuis, M. Lindmark, E. Lucero, D. Lyakh, S. Mandrà, J. R. McClean, M. McEwen, A. Megrant, X. Mi, K. Michielsen, M. Mohseni, J. Mutus, O. Naaman, M. Neeley, C. Neill, M. Y. Niu, E. Ostby, A. Petukhov, J. C. Platt, C. Quintana, E. G. Rieffel, P. Roushan, N. C. Rubin, D. Sank, K. J. Satzinger, V. Smelyanskiy, K. J. Sung, M. D. Trevithick, A. Vainsencher, B. Villalonga, T. White, Z. J. Yao, P. Yeh, A. Zalcman, H. Neven, and J. M. Martinis, Quantum supremacy using a programmable superconducting processor, Nature **574**, 505 (2019).
[36] A. Winick, J. J. Wallman, and J. Emerson, Simulating and mitigating crosstalk, Phys. Rev. Lett. **126**, 230502 (2021).
[37] R. Acharya, I. Aleiner, R. Allen, T. I. Andersen, M. Ansmann, F. Arute, K. Arya, A. Asfaw, J. Atalaya, R. Babbush, D. Bacon, J. C. Bardin, J. Basso, A. Bengtsson, S. Boixo, G. Bortoli, A. Bourassa, J. Bovaird, L. Brill, M. Broughton, B. B. Buckley, D. A. Buell, T. Burger, B. Burkett, N. Bushnell, Y. Chen, Z. Chen, B. Chiaro, J. Cogan, R. Collins, P. Conner, W. Courtney, A. L. Crook, B. Curtin, D. M. Debroy, A. Del Toro Barba, S. Demura, A. Dunsworth, D. Eppens, C. Erickson, L. Faoro, E. Farhi, R. Fatemi, L. Flores Burgos, E. Forati, A. G. Fowler, B. Foxen, W. Giang, C. Gidney, D. Gilboa, M. Giustina, A. Grajales Dau, J. A. Gross, S. Habegger, M. C. Hamilton, M. P. Harrigan, S. D. Harrington, O. Higgott, J. Hilton, M. Hoffmann, S. Hong, T. Huang, A. Huff, W. J. Huggins, L. B. Ioffe, S. V. Isakov, J. Iveland, E. Jeffrey, Z. Jiang, C. Jones, P. Juhas, D. Kafri, K. Kechedzhi, J. Kelly, T. Khattar, M. Khezri, M. Kieferová, S. Kim, A. Kitaev, P. V. Klimov, A. R. Klots, A. N. Korotkov, F. Kostritsa, J. M. Kreikebaum, D. Landhuis, P. Laptev, K.-M. Lau, L. Laws, J. Lee, K. Lee, B. J. Lester, A. Lill, W. Liu, A. Locharla, E. Lucero, F. D. Malone, J. Marshall, O. Martin, J. R. McClean, T. McCourt, M. McEwen, A. Megrant, B. Meurer Costa, X. Mi, K. C. Miao, M. Mohseni, S. Montazeri, A. Morvan, E. Mount, W. Mruczkiewicz, O. Naaman, M. Neeley, C. Neill, A. Nersisyan, H. Neven, M. Newman, J. H. Ng, A. Nguyen, M. Nguyen, M. Y. Niu, T. E. O'Brien, A. Opremcak, J. Platt, A. Petukhov, R. Potter, L. P. Pryadko, C. Quintana, P. Roushan, N. C. Rubin, N. Saei, D. Sank, K. Sankaragomathi, K. J. Satzinger, H. F. Schurkus, C. Schuster, M. J. Shearn, A. Shorter, V. Shvarts, J. Skruzny, V. Smelyanskiy, W. C. Smith, G. Sterling, D. Strain, M. Szalay, A. Torres, G. Vidal, B. Villalonga, C. Vollgraff Heidweiller, T. White, C. Xing, Z. J. Yao, P. Yeh, J. Yoo, G. Young, A. Zalcman, Y. Zhang, N. Zhu, and G. Q. AI, Suppressing quantum errors by

scaling a surface code logical qubit, Nature **614**, 676 (2023).

[38] S. J. Evered, D. Bluvstein, M. Kalinowski, S. Ebadi, T. Manovitz, H. Zhou, S. H. Li, A. A. Geim, T. T. Wang, N. Maskara, H. Levine, G. Semeghini, M. Greiner, V. Vuletić, and M. D. Lukin, High-fidelity parallel entangling gates on a neutral-atom quantum computer, Nature **622**, 268 (2023).

[39] H. Levine, A. Keesling, G. Semeghini, A. Omran, T. T. Wang, S. Ebadi, H. Bernien, M. Greiner, V. Vuletić, H. Pichler, and M. D. Lukin, Parallel implementation of high-fidelity multiqubit gates with neutral atoms, Phys. Rev. Lett. **123**, 170503 (2019).

[40] A. Pagano, S. Weber, D. Jaschke, T. Pfau, F. Meinert, S. Montangero, and H. P. Büchler, Error budgeting for a controlled-phase gate with strontium-88 rydberg atoms, Phys. Rev. Res. **4**, 033019 (2022).

[41] S. Bravyi and A. Kitaev, Universal quantum computation with ideal clifford gates and noisy ancillas, Phys. Rev. A **71**, 022316 (2005).

[42] E. Knill, Fault-tolerant postselected quantum computation: Schemes (2004), arXiv:quant-ph/0402171 [quant-ph].

[43] V. Tripathi, H. Chen, E. Levenson-Falk, and D. A. Lidar, Modeling low- and high-frequency noise in transmon qubits with resource-efficient measurement, PRX Quantum **5**, 010320 (2024).

[44] M. Rimbach-Russ, S. G. J. Philips, X. Xue, and L. M. K. Vandersypen, Simple framework for systematic high-fidelity gate operations, Quantum Science and Technology **8**, 045025 (2023).

[45] F. A. Calderon-Vargas and J. P. Kestner, Dynamically correcting a CNOT gate for any systematic logical error, Phys. Rev. Lett. **118**, 150502 (2017).

[46] J. Marshall, F. Wudarski, S. Hadfield, and T. Hogg, Characterizing local noise in qaoa circuits, IOP SciNotes **1**, 025208 (2020).